

Article

pH-Induced Modulation of *Vibrio fischeri* Population Life Cycle

Ana Rita Silva ^{1,2}, Cláudia Sousa ^{1,2}, Daniela Exner ³, Ruth Schwaiger ³, Maria Madalena Alves ¹, Dmitri Y. Petrovykh ^{2,*} and Luciana Pereira ¹

- ¹ CEB, Centre of Biological Engineering, University of Minho, 4710-057 Braga, Portugal; ana.rita.silva@ceb.uminho.pt (A.R.S.); claudiasousa@ceb.uminho.pt (C.S.); madalena.alves@deb.uminho.pt (M.M.A.); lucianapereira@deb.uminho.pt (L.P.)
- ² International Iberian Nanotechnology Laboratory, 4715-330 Braga, Portugal
- ³ Institute for Applied Materials, Karlsruhe Institute of Technology, 76344 Eggenstein-Leopoldshafen, Germany; daniela.exner@kit.edu (D.E.); r.schwaiger@fz-juelich.de (R.S.)
- * Correspondence: dmitri.petrovykh@inl.int

Abstract: Commonly used as biological chemosensors in toxicity assays, *Vibrio fischeri* bacteria were systematically characterized using complementary physicochemical and biological techniques to elucidate the evolution of their properties under varying environmental conditions. Changing the pH above or below the optimal pH 7 was used to model the long-term stress that would be experienced by *V. fischeri* in environmental toxicology assays. The spectral shape of bioluminescence and cell-surface charge during the exponential growth phase were largely unaffected by pH changes. The pH-induced modulation of *V. fischeri* growth, monitored via the optical density (OD), was moderate. In contrast, the concomitant changes in the time-profiles of their bioluminescence, which is used as the readout in assays, were more significant. Imaging at discrete timepoints by scanning electron microscopy (SEM) and helium-ion microscopy (HIM) revealed that mature *V. fischeri* cells maintained a rod-shaped morphology with the average length of $2.2 \pm 1 \mu\text{m}$ and diameter of $0.6 \pm 0.1 \mu\text{m}$. Detailed morphological analysis revealed subpopulations of rods having aspect ratios significantly larger than those of average individuals, suggesting the use of such elongated rods as an indicator of the multigenerational environmental stress. The observed modulation of bioluminescence and morphology supports the suitability of *V. fischeri* as biological chemosensors for both rapid and long-term assays, including under environmental conditions that can modify the physicochemical properties of novel anthropogenic pollutants, such as nanomaterials and especially stimulus-responsive nanomaterials.

Keywords: *Vibrio fischeri*; bioluminescence; cell-surface charge; scanning electron microscopy; helium-ion microscopy; zeta potential; cell morphology; cell-size distribution; environmental stress

Citation: Silva, A.R.; Sousa, C.; Exner, D.; Schwaiger, R.; Alves, M.M.; Petrovykh, D.Y.; Pereira, L. pH-Induced Modulation of *Vibrio fischeri* Population Life Cycle. *Chemosensors* **2021**, *9*, 283. <https://doi.org/10.3390/chemosensors9100283>

Academic Editors: Jana Drbohlavová and Agnieszka Mech

Received: 28 June 2021

Accepted: 1 October 2021

Published: 5 October 2021

Publisher's Note: MDPI stays neutral with regard to jurisdictional claims in published maps and institutional affiliations.



Copyright: © 2021 by the authors. Licensee MDPI, Basel, Switzerland. This article is an open access article distributed under the terms and conditions of the Creative Commons Attribution (CC BY) license (<https://creativecommons.org/licenses/by/4.0/>).

1. Introduction

For assessing environmental effects of anthropogenic pollutants, including nanomaterials, biological chemosensors, whereby the potential hazards posed by the material are evaluated based on monitoring the behavior of a bacterial population, offer an effective and practical solution [1–3]. The short life cycle and correspondingly rapid metabolism of bacteria that are used as biological chemosensors in toxicity assays, in particular, enable rapid assessment for acute toxicity of both soluble compounds [4,5] and samples containing solid materials (e.g., soil, waste, and sludge) [6].

Stimulus-responsive nanomaterials, also known as “smart” nanomaterials, are entering the market [7] in high-volume applications in agriculture [8], food [9], and cosmetics [10]. After the release of nanomaterials in these applications, their eventual fate often leads to accumulation in the soil [11] or aquatic environment [12], where bacterial chemosensors

are an important tool for assessment of ecotoxicity, because they are well suited for assays in complex natural environments and because bacteria play a significant role in the interaction of nanomaterials with ecosystems [12,13]. The responsive nanomaterials are also likely to participate in complex interactions with other nanomaterials, compounds, and ionic species that can strongly modulate the combined effect of such mixtures on biological systems [14]. In these complex environments, surface interactions play a particularly important role in modulating the toxic effects of the participating nanomaterials and compounds, as detected by bacterial assays [15]. The complexity of the underlying physicochemical phenomena highlights the need for an improved understanding of the effects that the variation of solution parameters can have on physicochemical and biological properties of the bacteria used in the assays.

As a model microorganism, the marine bacterium *Vibrio fischeri* from the Vibrionaceae family [16] is primarily studied due to the bioluminescence that naturally emerges in *V. fischeri* populations. In a normal life cycle, this bioluminescence is activated by quorum sensing in the exponential growth phase [17–20] and requires luciferase (and adenosine 5'-triphosphate, ATP) activity [21–23], thereby making *V. fischeri* populations a popular choice for model studies of quorum sensing [17,18,24–27] or bioluminescence modulation [22,28]. Rapid changes in the bioluminescence of *V. fischeri* populations are typically due to the modulation of the luciferase activity by the presence of stimulating or inhibiting substances or by environmental conditions, including temperature, oxygen concentration, and pH [22,28].

The convenience of the bioluminescence “readout” of their metabolic state, is the basis for using *V. fischeri* in bioassays [29,30]. The rapid and reproducible bioluminescence-inhibitory response in *V. fischeri* populations [22,31–35] led to its standardization in several commercially available kits [30,36–39].

In contrast to their widespread use in acute-toxicity assays, the response of *V. fischeri* populations to long-term environmental conditions is less well understood. We chose pH as a model environmental parameter to track the resulting long-term life-cycle and metabolic responses of *V. fischeri* cultures. In addition to being an important parameter subject to variations in natural environments, e.g., during ecotoxicity testing, particularly of responsive nanomaterials, pH represents a factor that can be systematically controlled in model experiments that elucidate the long-term environmental effects on both physicochemical and biological characteristics of *V. fischeri*. The emerging interest in using model *V. fischeri* populations in long-term bioassays, including under the environmental exposure to anthropogenic nanoparticles [40,41] that interact with microorganisms via both physicochemical and biological pathways [42–47], further highlights the practical importance of understanding the pH-dependent life cycle of *V. fischeri* populations. Accordingly, we used multiple complementary physicochemical and biological techniques to quantitatively follow the pH-dependent life cycles of *V. fischeri* populations via a combination of continuous and discrete timepoint measurements.

2. Materials and Methods

All the inorganic reagents used to prepare the media and solutions described in this section were of 98% or higher purity.

2.1. Organism and Growth Medium

V. fischeri strain NRRL-B-11177, commercially designated as “BioFix® Lumi luminous bacteria”, was obtained in freeze-dried form from Macherey-Nagel GmbH & Co. KG (Düren, Germany). The growth medium for bioluminescent bacteria was adapted from the standard protocol described in ISO 1134-1, “Water quality determination of the inhibitory effect of water samples on the light emission of *V. fischeri* (luminescent bacteria test)” [48,49].

The liquid growth medium was composed of peptic digest of animal tissue (CAS 91079-38-8, VWR) (5 g), yeast extract (CAS 8013-01-2, Fisher) (0.5 g), NaCl (CAS 7647-14-

5, Merck) (30 g), $\text{Na}_2\text{HPO}_4 \cdot 2\text{H}_2\text{O}$ (CAS 10028-24-7, Sigma) (6.10 g), KH_2PO_4 (CAS 7758-11-4, Panreac) (3.52 g), $\text{MgCl}_2 \cdot 7\text{H}_2\text{O}$ (CAS 10034-99-8, Panreac) (0.204 g), $\text{NH}_4\text{H}_2\text{PO}_4$ (CAS 7722-76-1, Merck) (0.7 g), and glycerol (CAS 56-81-5, Acros) (3 mL) per 1 L of distilled water. Solid medium for stock cultures had the same composition plus agar (CAS 9002-18-0, Panreac) ($12 \text{ g} \cdot \text{L}^{-1}$). The pH of the agar medium was adjusted to 7.0 ± 0.2 , with HCl (1 M) and NaOH (1 M) (HI 207 pH meter, HANNA Instruments). Sterilization was performed by autoclaving (Hiclave HV-25L, HMC) for 20 min at ca. 100 kPa and $121 \text{ }^\circ\text{C}$.

2.2. Aerobic Growth of *V. fischeri*

The freeze-dried commercial bacteria were reactivated by the addition of 1 mL of reconstitution solution (nontoxic ultrapure water), followed by manual shaking. After 5–10 min, the bacteria were plated in Petri dishes with solid growth medium and incubated for 3 days at $20 \text{ }^\circ\text{C}$. The luminescent colonies were identified in the dark by visual observation, transferred to Erlenmeyer flasks (250 mL) containing 50 mL of liquid growth medium, and incubated at $20 \pm 1 \text{ }^\circ\text{C}$ in an orbital shaker (Excella E24 Incubator Shaker, New Brunswick Scientific) at 180 rpm. After 2 days of incubation, the bacterial culture was centrifuged for 10 min at 7596 rpm (corresponding to $6000 \times g$ in Allegra 64R, Beckman Coulter centrifuge); the pellet was resuspended in 1 mL of the protective medium: D(+)-glucose monohydrate (CAS 14431-43-7, Acros) (66 g), NaCl (CAS 7647-14-5, Merck) (4 g), L-histidine (CAS 71-00-1, Sigma) (2 g), bovine serum albumin (CAS 9048-46-8, Sigma) (0.5 g). Aliquots (500 μL) of the resulting suspension were transferred to cryovials, with the addition of 500 μL of glycerol (CAS 56-81-5, Acros). The stock cultures were stored at $-80 \text{ }^\circ\text{C}$.

For monitoring the bacterial aerobic growth, *V. fischeri* stock was transferred from cryovials to the solid growth medium in Petri dishes and incubated for 3 days at $20 \pm 1 \text{ }^\circ\text{C}$. To produce a batch of planktonic culture, a luminescent colony, identified in the dark by visual observation, was inoculated in an Erlenmeyer flask (250 mL) containing 50 mL of growth medium and incubated at $20 \pm 1 \text{ }^\circ\text{C}$ in an orbital shaker (Excella E24 Incubator Shaker, New Brunswick Scientific) at 180 rpm.

Continuous monitoring of *V. fischeri* growth was carried out in 24-well cell-culture plates (flat-bottom nontreated polystyrene plates, CytoOne) placed in a microplate reader (Cytation3, BioTek). Each well was filled with 2 mL of the bacterial culture and measured continuously (in kinetic mode) for 70 h, with continuous shaking (355 rpm with amplitude of 4 mm) at $21 \pm 2 \text{ }^\circ\text{C}$. The light emission and the cell density (optical density, OD_{578}) were monitored as described by the ISO 1134-1 [48]. Three replicates were measured in parallel in different wells.

The influence of the pH of the culture medium on the bacteria growth was evaluated by performing experiments at different pH values (6, 7, and 8). The pH of the medium was adjusted with solutions of HCl (1 M) or NaOH (1 M).

The luminescence emission spectrum was recorded during the exponential phase, 24 h of bacteria growth, at pH 6, 7, or 8, in a microplate reader (Cytation3, BioTek), using a 96-well optical-bottom polymer-base black plate (Nalge Nunc International).

2.3. Morphological Analysis

V. fischeri morphology was observed by scanning electron microscopy (SEM) at different phases of the growth, corresponding to the lag phase (5 h), exponential phase (20 h and 24 h), stationary phase (53 h), and death phase (117 h). To prepare samples for SEM at each timepoint, aliquots from batch-grown bacterial cultures were centrifuged for 5 min at 7596 rpm (corresponding to $6000 \times g$ in Allegra 64R, Beckman Coulter centrifuge), the supernatants were discarded, and the cells washed twice by centrifugation in artificial seawater (ASW). ASW was composed of NaCl (CAS 7647-14-5, Merck) (28.0 g), $\text{MgCl}_2 \cdot 6\text{H}_2\text{O}$ (CAS 7791-18-6, Acros) (5.0 g), $\text{MgSO}_4 \cdot 7\text{H}_2\text{O}$ (CAS 10034-99-8, Panreac) (4.5 g), $\text{CaCl}_2 \cdot 2\text{H}_2\text{O}$ (CAS 10035-04-8, Panreac) (1.5 g), and KCl (CAS 7447-40-7, Panreac) (0.8 g) per 1 L of ultrapure water [28]. After the two washes, the pellets were resuspended in ASW, and the OD was adjusted to 0.2. Then, 3 mL of the bacterial suspension was filtered

through a 0.2 µm polycarbonate filter (Whatman), and the filter was placed in a well of a six-well plate containing 3 mL of 2.5% solution of glutaraldehyde (CAS 111-30-8, Sigma) in 0.1 M sodium cacodylate buffer (CAS 6131-99-3, Sigma) at pH 7.3. The filter was kept in the well for 16 h at 4 °C, to fix the bacteria. After the fixation step, the filter was washed with sodium cacodylate buffer (CAS 6131-99-3, Sigma) three times for 10 min in each step. Then, the cells in the filter were dehydrated in a series of ethanol solutions (30%, 50%, 70%, 80%, 90%, 96%, and 100%), for 10 min in each solution. Ethanol-dried samples in 100% ethanol were placed in the critical-point dryer (Leica EM CPD300) for a critical-CO₂ drying sequence lasting 2 h.

To minimize imaging artifacts [50], SEM images were acquired in a field-emission SEM (Quanta 650 FEG, FEI), in low-vacuum mode, using the low-kV pressure-limiting aperture (PLA) cone for an operating voltage of 1.5 kV, at 5 mm working distance. The distributions of lengths and diameters for 300 bacteria were obtained via SEM image analysis in ImageJ software.

The morphology of *V. fischeri* in the exponential phase (24 h of growth) was also observed by helium-ion microscopy (HIM). The samples were investigated using a microscope (Orion NanoFab, Zeiss) equipped with an Everhart–Thornley detector for secondary electron collection. The images were acquired at an acceleration voltage of 25 kV, a beam current of 0.3 pA, and a working distance of 9 mm. The samples were imaged without conductive coatings; an electron flood gun was used to compensate for sample charging caused by the helium-ion beam.

2.4. Viability of *V. fischeri* Cells

The quantification of live bacteria was performed by colony-forming unit (CFU) counting. After 24 h of growth in liquid culture, the bacterial culture was 1:5 serially diluted in the growth medium; 100 µL aliquots of the diluted samples, corresponding to the dilution factors of 1.28×10^{-5} , 2.56×10^{-6} , 5.12×10^{-7} , and 1.02×10^{-7} , were transferred to Petri dishes containing solid growth medium (each with three replicates). Three assays were performed on different days, and the initial concentration was adjusted to $OD_{578} \approx 1.0 \pm 0.2$. The spreading of diluted bacterial culture was performed with sterile glass beads, manually shaking during 5 min. Plates were then incubated for 3 days at 20 ± 1 °C, and the estimation of bacterial abundance in the suspensions was performed by direct counts of CFUs. Confidence intervals (CI) of mean values were calculated using the statistical package of Microsoft Excel 2010, assuming the Student's *t*-distribution with $n > 30$ replicates. The CIs are reported at 95% confidence level (CL) as the mean $\pm 1.96 \cdot s/\sqrt{n}$ (s = standard deviation).

2.5. Characterization of Surface Charge

Zeta (ζ) potentials of the bacteria were measured in a Zetasizer NANO ZS-ZEN3600 (Malvern Instruments Limited, UK), equipped with an He–Ne laser (wavelength of 633 nm) and operating with a detection angle set to 173° (backscatter detection). The ζ -potentials were evaluated in two different assays. In the first assay, the cultures were grown at different pH (6, 7, and 8) for 24 h and measured in ultrapure water. Small amounts of HCl (1 M) or NaOH (1 M) were added to adjust the pH of the growth medium. After growth, the medium containing the bacteria was centrifuged for 5 min at 7596 rpm (corresponding to $6000 \times g$ in Allegra 64R, Beckman Coulter centrifuge), at 20 °C, and the pellet was resuspended in 15 mL of ultrapure water. In the second assay, the bacteria were grown during 24 h under the standard conditions at pH 7, then centrifuged and resuspended as described above. Before measurements, samples in water were adjusted to pH 6, 6.5, 7, 7.5, or 8 with HCl (1 M) or NaOH (1 M). The average value and standard deviation for each sample were obtained from 10 measurements at 25 °C. The results were obtained using the Smoluchowski theory approximation. Zetasizer 7 software (Malvern Instruments Limited, UK) was used to estimate ζ -potential values for bacteria.

3. Results

3.1. Dependence of *V. fischeri* Growth and Bioluminescence on pH

At the ISO-recommended optimal pH value of 7 [28,48,49,51], the lag phase of 6 h after inoculation was followed by the exponential phase until 28 h of growth, reaching the maximum OD of 1.9 in the stationary phase (Figure 1A). Previous reports [28,49] have established that bioluminescence of *V. fischeri* is strongly attenuated outside the range of pH 6 to pH 9. Because the attenuation of bioluminescence is the basis for using *V. fischeri* in toxicity assays, to limit the effect of the medium to a range of pH where the bioluminescence readings may be considered reliable, we limited the pH adjustment to one unit above or below the optimal value of pH 7. The effects of changing the pH of the growth medium were significantly different at pH 6 and pH 8 (Figure 1A). At pH 8, the lag and exponential phases were similar to those observed at pH 7 up to 18 h of growth. This earlier onset of the stationary phase at pH 8 resulted in a decreased maximum OD of 1.6, an 11% drop from the maximum at pH 7. In contrast, at pH 6, the growth rate in the exponential phase was significantly lower than that at the higher pH values, and the maximum OD reached in the stationary phase was only 1.3, a 37% drop from the maximum at pH 7. Even in this simple example of using pH as a model environmental parameter, the continuous monitoring helped to reveal both similarities and divergences among the three growth curves [52,53], the exact timing of which could be missed in measurements at discrete timepoints.

In the time-profile of the bioluminescence intensity, two peaks—initial at 17 h and secondary at 28 h—were observed during growth at the optimal pH 7 and at pH 8 (Figure 1B). In contrast to the correlated time-profiles of bioluminescence at both higher pH values, a single peak at 25 h was observed during growth at pH 6 (Figure 1B). The visible intensity differences of batch-grown cultures during the exponential phase (Figure S1A, Supplementary Materials) qualitatively matched those measured continuously in the 96-well plates (Figure 1B). Comparison of the bioluminescence spectra (Figure S1B) measured at pH 6, 7, and 8 revealed that the shapes of the spectral envelopes were similar under all three conditions.

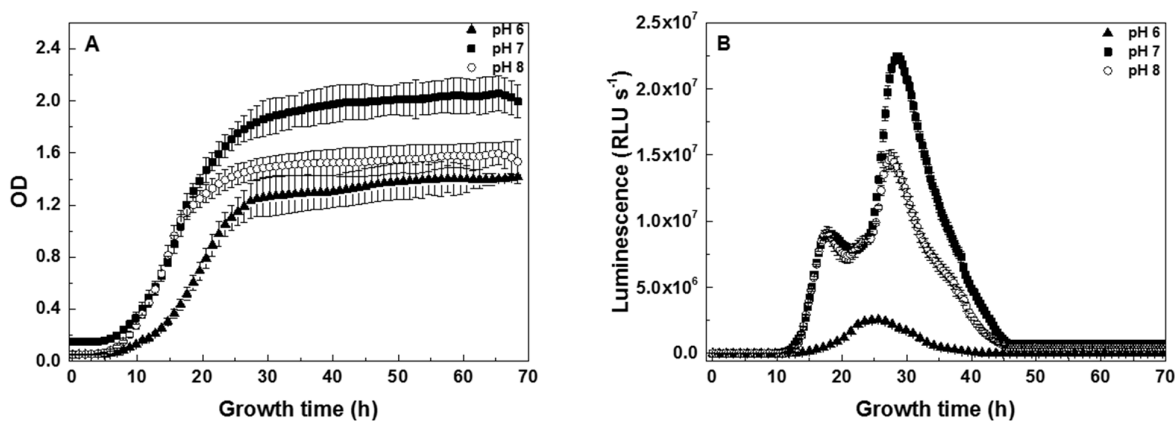


Figure 1. Continuous monitoring of *V. fischeri* aerobic growth at different pH. Data are shown with a different symbol for each of the three pH values and represent continuous measurements over 70 h of (A) optical density (OD) and (B) bioluminescence emission. Correlated initial (17 h) and secondary (28 h) peaks in bioluminescence are observed at pH 7 and 8, in contrast to a single peak (25 h) at pH 6.

3.2. Surface Charge Analysis

The surface charge of bacterial cells may depend on the pH of their environment. To model the conditions for both long-term and rapid pH-dependent assays, we measured

the surface charge of *V. fischeri* cells following two protocols summarized in Table 1. *V. fischeri* cells maintained a consistent surface charge independently of the pH-dependent protocol used, with the only exception of the surface charge observed for bacteria grown at pH 7 and resuspended at pH 6.

Table 1. Zeta-potential of *V. fischeri* grown under different pH conditions.

pH	Growth at Specified pH ¹ (ζ -potential, mV)	Exposed to Specified pH ² (ζ -potential, mV)
6	-40.8 ± 5.9	-18.0 ± 1.2
6.5	-	-37.9 ± 0.8
7	-44.5 ± 3.9	-38.9 ± 0.7
7.5	-	-37.5 ± 0.6
8	-45.8 ± 7.4	-38.4 ± 0.9

¹ Grown for 24 h in medium at the specified pH, then measured in water at pH 7. ² Grown for 24 h in medium at pH 7, then measured in water at the specified pH.

3.3. Viability Assays

Long-term growth-inhibition assays (Figure 1A) for *V. fischeri* were complemented by viability assays based on the CFU counting (Table S1, Supplementary Materials). The perfect correlation between the visible and bioluminescent colonies confirmed the presence of *V. fischeri* in each of the counted CFUs (Figure S2). The intrinsic variability of the viability under optimal growth conditions was directly examined by intra- and inter-assay comparison of the CFU counts (Table S1), which, according to the literature reports for other bacteria [54–56], indicated highly reproducible growth of our model *V. fischeri* cultures and consistency of setting the initial concentration via OD measurements ($OD_{578} \approx 1.0 \pm 0.2$).

3.4. Morphological Analysis

To investigate the normal evolution of *V. fischeri* cell morphology, we systematically analyzed by SEM imaging the size and shape distributions of *V. fischeri* bacteria at discrete timepoints throughout their full life cycle under optimal conditions (Figures 2, 3, and S3). In agreement with the exponential phase in the growth curve at pH 7 (Figure 1A), we observed clear evidence of active cell division (septa) at the 20 h and 24 h timepoints in Figure 2. Further morphological changes, including the emergence of extreme aspect ratios, were investigated by SEM (Figures 3, S3, and S4) and complementary HIM (Figure 4) imaging.

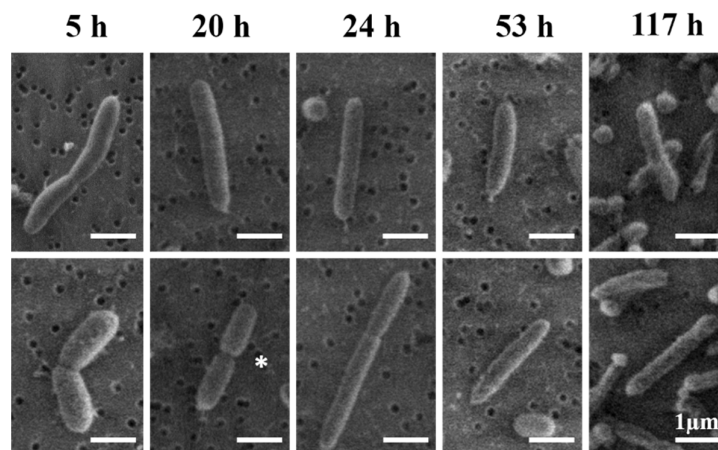


Figure 2. Scanning electron microscopy (SEM) images illustrating the cell division pattern throughout the life cycle of a *V. fischeri* population. The depicted timepoints correspond to the lag

(5 h), exponential (20 h and 24 h), stationary (53 h), and death (117 h) phases (see Figure 1A). The full-grown adult cells of ca. 2 μm length are observed at 53 h. Cells undergoing division are commonly observed only in the first two phases (5 h, 20 h, and 24 h); * clear example of a septum in the exponential phase (20 h). Dark round features in the background are ca. 0.2 μm pores in the supporting polycarbonate filter.

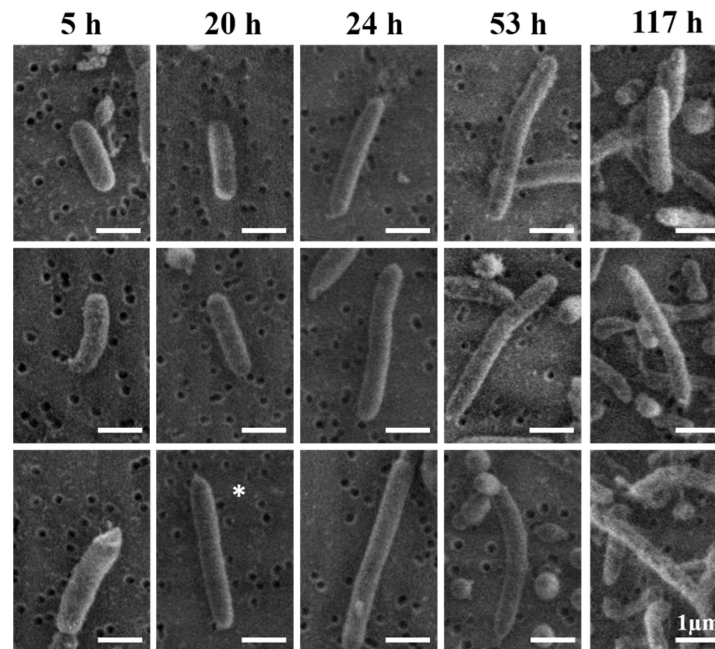


Figure 3. Emergence of the extended-rod morphology over the life cycle of *V. fischeri*. SEM images were acquired at five timepoints corresponding to the lag (5 h), exponential (20 h and 24 h), stationary (53 h), and death (117 h) phases (see Figure 1A). Panels at each timepoint illustrate that, starting from aspect ratios in the 3.5–4.0 range for normal adult individuals (ca. 2 μm in length), increasingly higher aspect ratios are observed for extended-rod morphologies as a function of increasing growth time; * clear example of a “double-length” extended-rod morphology in the exponential phase (20 h).

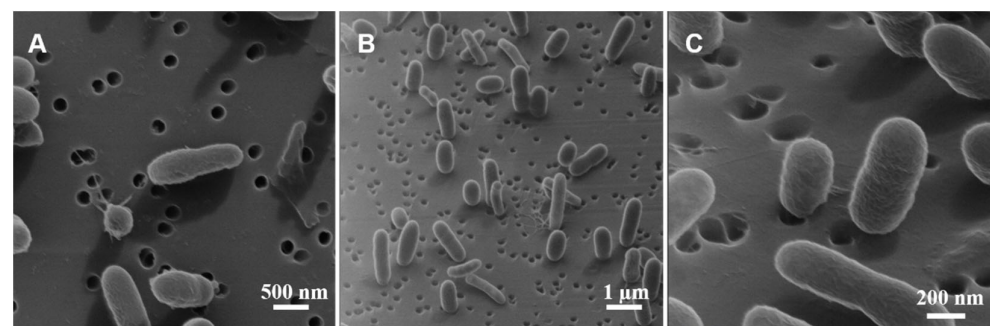


Figure 4. Helium-ion microscopy (HIM) images of *V. fischeri* in the exponential phase (24 h timepoint). Ambiguity in interpreting the cell morphology based on the top-down view (A) is resolved by tilting the stage 50° off-normal (B and C).

4. Discussion

4.1. Timing of the *V. fischeri* Growth Phases

The durations of the lag and exponential phases observed for *V. fischeri* in this work (Figure 1A) are in general agreement with the literature values, although some much shorter durations have also been reported. For an ES114 strain of *V. fischeri* from a host squid *Euprymna scolope*, the lag phase lasted 6 h, followed by the exponential phase for the

next 14–16 h [57]. For the same ES114 strain grown in the presence of trimethylamine *N*-oxide (TMAO), lag phases as short as 2 h and exponential phases as short as 2–4 h were observed [58], indicating that the duration of the growth phases is strongly condition- and stimulant-dependent. Similarly, in a continuous monitoring (based on OD₄₅₀) study of an unspecified cryopreserved strain of *V. fischeri*, typical duration of the lag phase was reported to be 2–3 h, with a broader range observed for the exponential phase (between 10 and 24 h), depending on the growth conditions [53]. Lastly, for the MJ1 strain, the reported lag phase duration was <3 h, with the exponential phase lasting until about 16–17 h [26].

4.2. Surface Charge of *V. fischeri* Is pH-Independent

The largely pH-independent ζ -potential values measured in this work (Table 1) are in good agreement with the -30.1 ± 9 mV previously reported for *V. fischeri* (DSM 507 strain) at pH 7.2 [59]. In particular, the near-constant surface charge observed for *V. fischeri* cells grown in the media at pH 6, 7, or 8, i.e., under conditions analogous to those of the long-term cell-growth and bioluminescence measurements in Figure 1, implies that the suppressed growth at pH 6 did not result from dramatic changes in the electrostatic environment of cell surfaces. In terms of bioassay applications, the consistent surface charge of *V. fischeri* is beneficial for measurements at varying pH, whereby the pH of the environment would modulate the ζ -potential values of nanomaterials being tested for toxicity, but not the surface charge of the cells used as bioluminescent chemo/bio sensors.

4.3. Time-Profiles of *V. fischeri* Bioluminescence Are pH-Dependent

Superficially, the dramatic differences between the time-dependent bioluminescence profiles measured at pH 6, 7, and 8 (Figure 1B) may suggest that the environmental pH significantly affects the bioluminescence of individual *V. fischeri* cells. The largely pH-independent cell-surface charge (Table 1) and spectral shapes of the bioluminescence (Figure S1B), however, indicate that the pH effects apparent in Figure 1B are not the result of directly affecting bioluminescent centers, but rather are largely indirect. Specifically, the time-dependent peaks in bioluminescence are correlated with parameters of the corresponding pH-dependent growth curves (Figure 1A) coupled with a quorum-sensing mechanism.

The timing of the initial peak in bioluminescence, i.e., the initial peak at ca. 17 h for pH 7 and 8 or the single peak at ca. 25 h for pH 6, is determined by the initial production among the growing population of the quorum-sensing agent acyl homoserine lactone (AHL), which is known to be an autoinductor for expression of the bioluminescent luciferase in *V. fischeri* [24,25]. Both the timing (via AHL concentration) and the intensity of the initial peak in bioluminescence, therefore, are proportional to the cell density, in agreement with the data in Figure 1. The exponential phases behaved almost identically at pH 7 and 8 (Figure 1A); therefore, both populations reached the threshold cell density for AHL expression at nearly the same time (before 17 h) and near-identical cell densities at 17 h, resulting in the almost identical timing and intensity of the initial peaks in bioluminescence at pH 7 and 8 (Figure 1B). Conversely, the exponential phase at pH 6 was delayed and had a slower growth rate compared to those at pH 7 and 8 (Figure 1A); therefore, the threshold cell density for AHL expression was also delayed, and the initial peak in bioluminescence at pH 6 was pushed back to 25 h (Figure 1B). Furthermore, the lowest cell density (Figure 1A) reached at pH 6 resulted in the lowest intensity of the bioluminescence peak (Figures 1B and S1).

For the secondary bioluminescence peaks at pH 7 and 8 (Figure 1B), both the correlated delay to ca. 28 h and the intensities relative to those of the initial peaks are consistent with the modeling predictions of the time-dependent concentration of AHL in a medium during bacterial growth past the initial threshold for AHL expression [60]. In direct analogy with the initial peaks, the intensity of the secondary peaks correlated with the corresponding cell density (Figure 1A), resulting in the lower intensity observed at pH 8 than at pH 7 (Figure 1B). In further agreement with the modeling predictions [60], because the

initial peak in bioluminescence at pH 6 coincided with the end of the exponential growth phase (see Figure 1A,B), there was no continued increase in cell density to support a secondary delayed peak; thus, it never emerged at pH 6 (Figure 1B).

4.4. Typical Morphology of *V. fischeri* Cells

The distributions of lengths and diameters of *V. fischeri* bacteria (Table 2) were estimated for each of the discrete timepoints characterized by SEM. Averaged over all the growth phases, the mean length of the rod-shaped cells was $2.2 \pm 1 \mu\text{m}$, in good agreement with the length of adult individuals observed in the stationary phase, e.g., at the 53 h timepoint in Figure 2. While there were small variations in the mean values estimated at different timepoints, the differences among them were not statistically significant. The notably higher mean and uncertainty ($3.3 \pm 2 \mu\text{m}$) estimated for the 5 h timepoint was primarily the result of the low bacterial density and, thus, their low total number in SEM images at that early stage of growth. The observed variations in the mean diameter values were not statistically significant among the timepoints, with an overall mean diameter of $0.6 \pm 0.1 \mu\text{m}$.

Table 2. Distributions of length and diameter of *V. fischeri* throughout the life cycle.

Growth Time (h)	Length (μm)	Diameter (μm)
5	3.2 ± 1.9	0.59 ± 0.1
20	2.2 ± 1.0	0.63 ± 0.1
24	1.9 ± 0.6	0.59 ± 0.1
53	2.1 ± 0.9	0.59 ± 0.1
117	2.1 ± 0.8	0.53 ± 0.1
Average	2.2 ± 1	0.6 ± 0.1

The mean length observed in this work was at the lower and upper limits, respectively, of the previous literature values for *V. fischeri* cells measured using optical microscopy ($2\text{--}3 \mu\text{m}$) [27,32] and SEM ($1.5\text{--}2 \mu\text{m}$) [59]. The overall larger values obtained using optical microscopy were likely due to the shrinking of bacterial cells that commonly results from their preparation for SEM imaging, which includes fixation with glutaraldehyde and dehydration in ethanol and in the critical-point dryer [61].

Apart from this putative shrinking, our preparation protocol did not introduce major artefacts into the observed morphology of *V. fischeri* cells. The consistent mean diameter observed in this work, with an overall variability lower than that of the mean length (Table 2), for example, implies that the collapse of cell membranes during sample preparation was largely avoided. Furthermore, visualization of the individual flagella at the 24 h timepoint (Figure S5), in agreement with previous observations by transmission electron microscopy [62], indicates that the sample preparation and imaging protocols used in this work were sufficiently mild to preserve fine morphological features of *V. fischeri* cells. This validation of our experimental protocols supports the interpretation of morphological changes, such as lysed cells at 117 h in Figures S3 and S4, as being related to and representative of the bacterial population life cycle.

4.5. Interpretation of the Apparently Round Cell Morphology

In SEM images with high densities of *V. fischeri* cells (53 and 117 h timepoints in Figures 2, 3, S3, and S4), an apparently round cell morphology was very common. Elucidating the nature of this morphology of *V. fischeri* cells is important because, for other *Vibrio* species, the round-cell morphology with ca. $0.6 \mu\text{m}$ diameter has been reported specifically for bacteria in a viable but nonculturable (VBNC) state [63–65].

For *V. fischeri* cells, however, a close inspection of the shading around these apparently round features in SEM images (53 h timepoint in Figures S3 and S4) suggested that

they did not correspond to an actual spherical morphology. To reveal the true three-dimensional cell morphology corresponding to these apparently round features in SEM images, we performed complementary high-resolution imaging by HIM [66], which employs a helium-ion beam with a small convergence angle [67] to extend the depth of field 5–10 times beyond that of SEM [68]. HIM images acquired in a top-down view (Figure 4A) were similar to SEM ones (53 h timepoint in Figures 2, 3, S3, and S4), including an apparently round feature (lower-left quadrant of Figure 4A), but off-normal angle HIM images clearly and directly showed these features to be rod-shaped *V. fischeri* cells attached to the support in a nearly perpendicular orientation (Figure 4B,C). Accordingly, the above statistical analysis of bacterial lengths (Table 2) applied only to the subpopulation of the rod-shaped bacteria for which the flat orientation on the support was clear in SEM images.

4.6. Mechanism for Producing the Extended-Rod Morphology

The consistent mean length and diameter values throughout the entire life cycle of *V. fischeri* (Table 2) provided an estimate of a mean aspect ratio as ca. 3.7, which was similar to the aspect ratio observed for cells identified in SEM images as adult individuals, e.g., stationary cells at 53 h timepoint in Figure 2. A small fraction of the cells at each timepoint starting from 20 h, however, exhibited an extended-rod morphology with aspect ratios >4 (Figures 3 and S3–S5). Notably, these extended rods were typically about 2–3 times longer than statistically-average individual cells at the same timepoints (a “double-length” example is highlighted in Figure 3). Another yet smaller but distinct subpopulation of extra-long rods with lengths >10 μm could be identified at the 53 h and 117 h timepoints (Figures S3 and S4).

Considering the main bacterial growth mechanisms [69], the extended and extra-long rod minority subpopulations of *V. fischeri* with the observed characteristics can naturally emerge only in growth by cylindrical elongation and not by cell-tip extension. In the prototypical rod-shaped *Escherichia coli*, for example, extended and extra-long rod morphologies have previously been produced by cylindrical elongation from cells growing with suppressed division [69–71]. In our *V. fischeri* cultures, however, the double- and triple-length extended rods were much more frequent than the extra-long rods, pointing to discrete failures, rather than continuous suppression, of cell division as the most likely mechanism. Discrete failures should naturally produce many double- and triple-length individuals but few extra-long ones, because, for a given individual, the length would be determined not by the total growth time, but rather by the number of successive failed discrete divisions of its progenitor, i.e., by a mechanism exponentially suppressing extra-long rods. For example, in *E. coli* studies that employed cephalixin-induced, i.e., continuous, suppression of cell division, extended rods from an earlier timepoint became continuously longer with time [52,71], whereas, in our *V. fischeri* cultures, most of the extended rods never became extra-long at later timepoints (Figures S3 and S4).

4.7. Extended-Rod Morphology as a Metabolic Stress Indicator

Limited images from previous studies have shown normal *V. fischeri* populations as either exclusively short rods [62,63] or a mixture of short and extended rods similar to ours [52]. The latter study, in particular, correlated the elongated morphologies of bacteria to their growth under starvation conditions [52]. Accordingly, our extensive SEM imaging of a long-term *V. fischeri* culture provides the critical baseline statistics for use of the morphological distribution as a robust indicator of the long-term multigenerational environmental stress in environmental (eco)toxicology assays based on *V. fischeri*.

5. Conclusions

We systematically investigated the physicochemical and biological properties of *V. fischeri* bacteria to elucidate their compatibility with requirements for use in evaluating

long-term environmental (eco)toxicity of novel anthropogenic pollutants, including nano-materials and stimulus-responsive nanomaterials. Specifically, we investigated the pH-dependent growth, bioluminescence, and surface charge throughout the full life cycle of model *V. fischeri* populations.

We found that the pH of a *V. fischeri* culture medium, in the range between pH 6 and 8, primarily affects the growth of the *V. fischeri* population, which, in turn, modifies the time-profiles of bioluminescence. For applications of *V. fischeri* in both rapid and long-term bioluminescent-output bioassays, the pH-independent spectral shape of their bioluminescence and the nearly pH-independent ζ -potential provide validation of *V. fischeri* as a robust model microorganism. Particularly beneficial is the possibility to perform the *V. fischeri* assays in the practically important range of pH 6 to pH 8 without having to introduce “confounding factors” [72] to adjust the pH. For testing nanomaterials that change their surface charge significantly in this pH range, it is also useful to have model bacteria that maintain their surface charge, so that the testing predominantly reflects the physico-chemical effect of the pH on the nanomaterials and not on the bacterial chemosensor.

To evaluate the long-term effects of novel anthropogenic pollutants, bioassays based on bioluminescence can be complemented by morphological analyses of rod-shaped *V. fischeri* cells, whereby significant changes in the nature and frequency of the extended-rod morphologies—defined as being longer than the $2.2 \pm 1 \mu\text{m}$ average size and having an aspect ratio greater than 4—can be used as a robust indicator of the long-term multigenerational environmental stress in *V. fischeri* populations.

Supplementary Materials: The following are available online at www.mdpi.com/article/10.3390/chemosensors9100283/s1: Figure S1. Comparison of *V. fischeri* bioluminescence emission at different pH; Table S1. Viability assays for *V. fischeri*; Figure S2. Plates with a dilution series of *V. fischeri* for CFU counting; Figure S3. SEM images illustrating morphological changes throughout the life cycle of a *V. fischeri* population; Figure S4. SEM image of *V. fischeri* in the stationary phase (53 h timepoint); Figure S5: SEM image of *V. fischeri* in the exponential phase (24 h timepoint).

Author Contributions: Conceptualization, A.R.S. and D.Y.P.; methodology, A.R.S., C.S., L.P., and D.Y.P.; validation, A.R.S., C.S., and D.Y.P.; formal analysis, A.R.S. and C.S.; investigation, A.R.S., C.S., D.E., R.S., D.Y.P., and L.P.; resources, R.S., D.Y.P., and L.P.; writing—original draft preparation, A.R.S.; writing—review and editing, C.S., R.S., M.M.A., D.Y.P., and L.P.; supervision, M.M.A., D.Y.P., and L.P. All authors have read and agreed to the published version of the manuscript.

Funding: This study was supported by the Portuguese Foundation for Science and Technology (FCT) under the scope of the strategic funding of UIDB/04469/2020 unit and COMPETE 2020 (POCI-01-0145-FEDER-006684) and BioTecNorte operation (NORTE-01-0145-FEDER-000004) funded by European Regional Development Fund under the scope of Norte2020 Programa Operacional Regional do Norte. A.R.S. holds an FCT fellowship SFRH/BD/131905/2017. Measurements using the helium-ion microscope were supported by the Karlsruhe Nano Micro Facility (KNMF) of the Karlsruhe Institute of Technology (KIT) under projects 2016-015-010689 and 2018-019-021475.

Institutional Review Board Statement: Not applicable.

Institutional Review Board Statement: Not applicable.

Data Availability Statement: Data are contained within the article or Supplementary Materials.

Acknowledgments: The authors acknowledge Pedro Martins (University of Minho) for the support in the surface charge and bacteria life cycle analysis.

Conflicts of Interest: The authors declare no conflicts of interest. The funders had no role in the design of the study; in the collection, analyses, or interpretation of data; in the writing of the manuscript, or in the decision to publish the results.

References

1. Abbas, M.; Adil, M.; Ehtisham-ul-Haque, S.; Munir, B.; Yameen, M.; Ghaffar, A.; Shar, G.A.; Asif Tahir, M.; Iqbal, M. *Vibrio fischeri* bioluminescence inhibition assay for ecotoxicity assessment: A review. *Sci. Total Environ.* **2018**, *626*, 1295–1309, doi:10.1016/j.scitotenv.2018.01.066.

2. Kharkova, A.S.; Arlyapov, V.A.; Turovskaya, A.D.; Shvets, V.I.; Reshetilov, A.N. A mediator microbial biosensor for assaying general toxicity. *Enzym. Microb. Technol.* **2020**, *132*, 109435, doi:10.1016/j.enzmictec.2019.109435.
3. Mirjani, M.; Soleimani, M.; Salari, V. Toxicity assessment of total petroleum hydrocarbons in aquatic environments using the bioluminescent bacterium *Aliivibrio fischeri*. *Ecotoxicol. Environ. Saf.* **2021**, *207*, 111554, doi:10.1016/j.ecoenv.2020.111554.
4. Parvez, S.; Venkataraman, C.; Mukherji, S. A review on advantages of implementing luminescence inhibition test (*Vibrio fischeri*) for acute toxicity prediction of chemicals. *Environ. Int.* **2006**, *32*, 265–268.
5. Asano, T.; Wang, P.C.; Iwasaki, A. Spectrophotometric detection of labile zinc (II) released from metallothionein: A simple method to evaluate heavy metal toxicity. *J. Biosci. Bioeng.* **2010**, *109*, 638–644, doi:10.1016/j.jbiosc.2009.11.016.
6. Mendonça, E.; Picado, A.; Paixão, S.M.; Silva, L.; Cunha, M.A.; Leitão, S.; Moura, I.; Cortez, C.; Brito, F. Ecotoxicity tests in the environmental analysis of wastewater treatment plants: Case study in Portugal. *J. Hazard. Mater.* **2009**, *163*, 665–670, doi:10.1016/j.jhazmat.2008.07.012.
7. Gottardo, S.; Mech, A.; Drbohlavová, J.; Malyska, A.; Bøwadt, S.; Riego Sintes, J.; Rauscher, H. Towards safe and sustainable innovation in nanotechnology: State-of-play for smart nanomaterials. *NanoImpact* **2021**, *21*, 100297, doi:10.1016/j.nanoimp.2021.100297.
8. Grillo, R.; Mattos, B.D.; Antunes, D.R.; Forini, M.M.L.; Monikh, F.A.; Rojas, O.J. Foliage adhesion and interactions with particulate delivery systems for plant nanobionics and intelligent agriculture. *Nano Today* **2021**, *37*, 101078, doi:10.1016/j.nantod.2021.101078.
9. Karimi, M.; Sadeghi, R.; Kokini, J. Human exposure to nanoparticles through trophic transfer and the biosafety concerns that nanoparticle-contaminated foods pose to consumers. *Trends Food Sci. Technol.* **2018**, *75*, 129–145, doi:10.1016/j.tifs.2018.03.012.
10. Fytianos, G.; Rahdar, A.; Kyzas, G.Z. Nanomaterials in cosmetics: Recent updates. *Nanomaterials* **2020**, *10*, 979, doi:10.3390/nano10050979.
11. Rodrigues, S.M.; Trindade, T.; Duarte, A.C.; Pereira, E.; Koopmans, G.F.; Römkens, P.F.A.M. A framework to measure the availability of engineered nanoparticles in soils: Trends in soil tests and analytical tools. *TrAC Trends Anal. Chem.* **2016**, *75*, 129–140, doi:10.1016/j.trac.2015.07.003.
12. Németh, I.; Molnár, S.; Vaszita, E.; Molnár, M. The Biolog EcoPlate™ technique for assessing the effect of metal oxide nanoparticles on freshwater microbial communities. *Nanomaterials* **2021**, *11*, 1777, doi:10.3390/nano11071777.
13. Fekete-Kertész, I.; Piszman, D.; Molnár, M. Particle size and concentration dependent ecotoxicity of nano- and microscale TiO₂—Comparative study by different aquatic test organisms of different trophic levels. *Water Air Soil Pollut.* **2017**, *228*, 245, doi:10.1007/s11270-017-3394-5.
14. Trinh, T.X.; Kim, J. Status Quo in data availability and predictive models of nano-mixture toxicity. *Nanomaterials* **2021**, *11*, 124, doi:10.3390/nano11010124.
15. Ríos, F.; Fernández-Arteaga, A.; Fernández-Serrano, M.; Jurado, E.; Lechuga, M. Silica micro- and nanoparticles reduce the toxicity of surfactant solutions. *J. Hazard. Mater.* **2018**, *353*, 436–443, doi:10.1016/j.jhazmat.2018.04.040.
16. Urbanczyk, H.; Ast, J.C.; Higgins, M.J.; Carson, J.; Dunlap, P. V. Reclassification of *Vibrio fischeri*, *Vibrio logei*, *Vibrio salmonicida* and *Vibrio wodanis* as *Aliivibrio fischeri* gen. nov., comb. nov., *Aliivibrio logei* comb. nov., *Aliivibrio salmonicida* comb. nov. and *Aliivibrio wodanis* comb. nov. *Int. J. Syst. Evol. Microbiol.* **2007**, *57*, 2823–2829, doi:10.1099/ijs.0.65081-0.
17. Kimura, Y.; Tashiro, Y.; Saito, K.; Kawai-Noma, S.; Umeno, D. Directed evolution of *Vibrio fischeri* LuxR signal sensitivity. *J. Biosci. Bioeng.* **2016**, *122*, 533–538, doi:10.1016/j.jbiosc.2016.04.010.
18. Fuqua, W.C.; Winans, C.S.; Greenberg, E.P. Quorum sensing in bacteria: The LuxR-LuxI family of cell density-responsive transcriptional regulators. *J. Bacteriol.* **1994**, *176*, 269–275.
19. Madden, D.; Lidesten, B.-M. Bacterial illumination Culturing luminous bacteria. In *Bioscience Explained*; NCBE, The University of Reading: Reading, United Kingdom, 2001; Volume 1, pp. 1–8.
20. Neilson, K.H.; Platt, T.; Hastings, J.W. Cellular control of the synthesis and activity of the bacterial luminescent system. *J. Bacteriol.* **1970**, *104*, 313–322.
21. Kaiser, K.L.E. Correlations of *Vibrio fischeri* bacteria test data with bioassay data for other organisms. *Environ. Health Perspect.* **1998**, *106*, 583–591.
22. Dunn, A.K. *Vibrio fischeri* metabolism: Symbiosis and beyond. *Adv. Microb. Physiol.* **2012**, *61*, 37–68, doi:10.1016/B978-0-12-394423-8.00002-0.
23. Bose, J.L.; Kim, U.; Bartkowski, W.; Gunsalus, R.P.; Overley, A.M.; Lyell, N.L.; Visick, K.L.; Stabb, E.V. Bioluminescence in *Vibrio fischeri* is controlled by the redox-responsive regulator ArcA. *Mol. Microbiol.* **2007**, *65*, 538–553, doi:10.1111/j.1365-2958.2007.05809.x.
24. Li, Y.-H.; Tian, X. Quorum sensing and bacterial social interactions in biofilms. *Sensors* **2012**, *12*, 2519–2538, doi:10.3390/s120302519.
25. Lupp, C.; Ruby, E.G. *Vibrio fischeri* uses two quorum-sensing systems for the regulation of early and late colonization factors. *J. Bacteriol.* **2005**, *187*, 3620–3629, doi:10.1128/JB.187.11.3620.
26. Manefield, M.; Chong, G. Quorum Sensing signal synthesis may represent a selective advantage independent of its role in regulation of bioluminescence in *Vibrio fischeri*. *PLoS ONE* **2013**, *8*, e6744, doi:10.1371/journal.pone.0067443.
27. Pérez, P.D.; Hagen, S.J. Heterogeneous response to a quorum-sensing signal in the luminescence of individual *Vibrio fischeri*. *PLoS ONE* **2010**, *5*, e15473, doi:10.1371/journal.pone.0015473.

28. Scheerer, S.; Gomez, F.; Lloyd, D. Bioluminescence of *Vibrio fischeri* in continuous culture: Optimal conditions for stability and intensity of photoemission. *J. Microbiol. Methods* **2006**, *67*, 321–329, doi:10.1016/j.mimet.2006.04.010.
29. Rizzo, L. Bioassays as a tool for evaluating advanced oxidation processes in water and wastewater treatment. *Water Res.* **2011**, *45*, 4311–4340, doi:10.1016/j.watres.2011.05.035.
30. Marugán, J.; Bru, D.; Pablos, C.; Catalá, M. Comparative evaluation of acute toxicity by *Vibrio fischeri* and fern spore based bioassays in the follow-up of toxic chemicals degradation by photocatalysis. *J. Hazard. Mater.* **2012**, *213–214*, 117–122, doi:10.1016/j.jhazmat.2012.01.075.
31. Miyashiro, T.; Ruby, E.G. Shedding light on bioluminescence regulation in *Vibrio fischeri*. *Mol. Microbiol.* **2013**, *84*, 795–806, doi:10.1111/j.1365-2958.2012.08065.x.Shedding.
32. Silva, A.R.; Martins, P.M.; Lanceros-Mendez, S.; Teixeira, S.; Carabineiro, S.A.C.; Kuehn, K.; Cuniberti, G.; Alves, M.M.; Pereira, L. Ciprofloxacin wastewater treated by UVA photocatalysis: Contribution of irradiated TiO₂ and ZnO nanoparticles on the final toxicity as assessed by *Vibrio fischeri*. *RSC Adv.* **2016**, *6*, 95494–95503, doi:10.1039/C6RA19202E.
33. Silva, A.R.; Soares, O.S.G.P.; Pereira, M.F.R.; Alves, M.M.; Pereira, L. Tailoring carbon nanotubes to enhance their efficiency as electron shuttle on the biological removal of acid orange 10 under anaerobic conditions. *Nanomaterials* **2020**, *10*, 2496, doi:10.3390/nano10122496.
34. Silva, A.R.; Cavaleiro, A.J.; Soares, O.S.G.P.; Braga, C.S.N.; Salvador, A.F.; Pereira, M.F.R.; Alves, M.M.; Pereira, L. Detoxification of ciprofloxacin in an anaerobic bioprocess supplemented with magnetic carbon nanotubes: contribution of adsorption and biodegradation mechanisms. *Int. J. Mol. Sci.* **2021**, *22*, 2932, doi:10.3390/ijms22062932.
35. Qi, X.; Liu, P.; Liang, P.; Hao, W.; Li, M.; Huang, X. Dual-signal-biosensor based on luminescent bacteria biofilm for real-time online alert of Cu (II) shock. *Biosens. Bioelectron.* **2019**, *142*, 111500, doi:10.1016/j.bios.2019.111500.
36. Parvez, S.; Venkataraman, C.; Mukherji, S. Toxicity assessment of organic pollutants: Reliability of bioluminescence inhibition assay and univariate QSAR models using freshly prepared *Vibrio fischeri*. *Toxicol. Vitro.* **2008**, *22*, 1806–1813, doi:10.1016/j.tiv.2008.07.011.
37. Bird, D.J.; Jennings, V.L.K.; Rayner-Brandes, M.H. Assessing chemical toxicity with the bioluminescent Photobacterium (*Vibrio fischeri*): A comparison of three commercial systems. *Water Res.* **2001**, *35*, 3448–3456.
38. Bayo, J.; Angosto, J.M.; Gómez-López, M.D. Ecotoxicological screening of reclaimed disinfected wastewater by *Vibrio fischeri* bioassay after a chlorination-dechlorination process. *J. Hazard. Mater.* **2009**, *172*, 166–171, doi:10.1016/j.jhazmat.2009.06.157.
39. Minetto, D.; Libralato, G.; Ghirardini, A.V. Ecotoxicity of engineered TiO₂ nanoparticles to saltwater organisms: An overview. *Environ. Int.* **2014**, *66*, 18–27, doi:10.1016/j.envint.2014.01.012.
40. Bystrzejewska-Piotrowska, G.; Golimowski, J.; Urban, P.L. Nanoparticles: Their potential toxicity, waste and environmental management. *Waste Manag.* **2009**, *29*, 2587–2595, doi:10.1016/j.wasman.2009.04.001.
41. Hussain, S.M.; Braydich-Stolle, L.K.; Schrand, A.M.; Murdock, R.C.; Yu, K.O.; Mattie, D.M.; Schlager, J.J. Toxicity evaluation for safe use of nanomaterials: Recent achievements and technical challenges. *Adv. Mater.* **2009**, *21*, 1549–1559, doi:10.1002/adma.200801395.
42. Neal, A.L. What can be inferred from bacterium–nanoparticle interactions about the potential consequences of environmental exposure to nanoparticles? *Ecotoxicology* **2008**, *17*, 362–371, doi:10.1007/s10646-008-0217-x.
43. Tartanson, M.-A.; Soussan, L.; Rivallin, M.; Pecastaings, S.; Chis, C.V.; Penaranda, D.; Roques, C.; Faur, C. Dynamic mechanisms of the bactericidal action of an Al₂O₃-TiO₂-Ag granular material on an *Escherichia coli* strain. *Appl. Environ. Microbiol.* **2015**, *81*, 7135–7142, doi:10.1128/AEM.01950-15.
44. Zhang, W.; Hughes, J.; Chen, Y. Impacts of hematite nanoparticle exposure on biomechanical, adhesive, and surface electrical properties of *Escherichia coli* cells. *Appl. Environ. Microbiol.* **2012**, *78*, 3905–3915, doi:10.1128/AEM.00193-12.
45. Gao, X.-L.; Shao, M.-F.; Xu, Y.-S.; Luo, Y.; Zhang, K.; Ouyang, F.; Li, J. Non-selective separation of bacterial cells with magnetic nanoparticles facilitated by varying surface charge. *Front. Microbiol.* **2016**, *7*, 1891, doi:10.3389/fmicb.2016.01891.
46. Westmeier, D.; Hahlbrock, A.; Reinhardt, C.; Fröhlich-Nowoisky, J.; Wessler, S.; Vallet, C.; Pöschl, U.; Knauer, S.K.; Stauber, R.H. Nanomaterial–microbe cross-talk: Physicochemical principles and (patho) biological consequences. *Chem. Soc. Rev.* **2018**, *47*, 5312–5337, doi:10.1039/C6CS00691D.
47. Kurvet, I.; Juganson, K.; Vija, H.; Sihtmäe, M.; Blinova, I.; Syvertsen-Wiig, G.; Kahru, A. Toxicity of nine (doped) rare earth metal oxides and respective individual metals to aquatic microorganisms *Vibrio fischeri* and *Tetrahymena thermophila*. *Materials* **2017**, *10*, 754, doi:10.3390/ma10070754.
48. ISO 11348-1 INTERNATIONAL STANDARD. *Water Quality—Determination of the Inhibitory Effect of Water Samples on the Light Emission of Vibrio fischeri (Luminescent Bacteria Test)—Part1: Method Using Freshly Prepared Bacteria*; ISO—International Organization for Standardization: Geneva, Switzerland, 1998.
49. ISO 11348-3 INTERNATIONAL STANDARD. *Water Quality—Determination of the Inhibitory Effect of Water Samples on The Light Emission of Vibrio fischeri (Luminescent Bacteria Test)—Part3: Method Using Freeze-Dried Bacteria*; ISO—International Organization for Standardization: Geneva, Switzerland, 2007.
50. Sousa, C.; Petrovykh, D.Y. Characterization of Bio-nanosystems. In *Advances in Processing Technologies for Bio-based Nanosystems in Food*; Ramos, O., Pereira, R., Cerqueira, M., Martins, J., Teixeira, J., Malcata, F., Vicente, A., Eds.; CRC Press: Boca Raton: FL, USA, 2019; pp. 271–306. ISBN: 9780128115169.
51. Waters, P.; Lloyd, D. Salt, pH and temperature dependencies of growth and bioluminescence of three species of luminous bacteria analysed on gradient plates. *Microbiology* **1985**, *131*, 2865–2869, doi:10.1099/00221287-131-11-2865.

52. Fulladosa, E.; Murat, J.C.; Villaescusa, I. Effect of cadmium (II), chromium (VI), and arsenic (V) on long-term viability- and growth-inhibition assays using *Vibrio fischeri* marine bacteria. *Arch. Environ. Contam. Toxicol.* **2005**, *49*, 299–306, doi:10.1007/s00244-004-0170-5.
53. Schmitz, R.P.H.; Eisentrager, A.; Dott, W. Miniaturized kinetic growth inhibition assays with *Vibrio fischeri* and *Pseudomonas putida* (application, validation and comparison). *J. Microbiol. Methods* **1998**, *31*, 159–166.
54. Pan, H.; Zhang, Y.; He, G.-X.; Katagori, N.; Chen, H. A comparison of conventional methods for the quantification of bacterial cells after exposure to metal oxide nanoparticles. *BMC Microbiol.* **2014**, *14*, 222, doi:10.1186/s12866-014-0222-6.
55. Hannig, C.; Hannig, M.; Rehmer, O.; Braun, G.; Hellwig, E.; Al-Ahmad, A. Fluorescence microscopic visualization and quantification of initial bacterial colonization on enamel in situ. *Arch. Oral Biol.* **2007**, *52*, 1048–1056, doi:10.1016/j.archoral-bio.2007.05.006.
56. Sousa, C.; Sequeira, D.; Kolen'ko, Y.V.; Pinto, I.M.; Petrovykh, D.Y. Analytical protocols for separation and electron microscopy of nanoparticles interacting with bacterial cells. *Anal. Chem.* **2015**, *87*, 4641–4648, doi:10.1021/ac503835a.
57. Foster, J.S.; Khodadad, C.L.M.; Ahrendt, S.R.; Parrish, M.L. Impact of simulated microgravity on the normal developmental time line of an animal-bacteria symbiosis. *Sci. Rep.* **2013**, *3*, 1340, doi:10.1038/srep01340.
58. Dunn, A.K.; Stabb, E.V. Genetic analysis of trimethylamine N-oxide reductases in the light organ symbiont *Vibrio fischeri* ES114. *J. Bacteriol.* **2008**, *190*, 5814–5823, doi:10.1128/JB.00227-08.
59. Ivanova, E.P.; Mitik-Dineva, N.; Mocanasi, R.C.; Murphy, S.; Wang, J.; van Riessen, G.; Crawford, R.J. *Vibrio fischeri* and *Escherichia coli* adhesion tendencies towards photolithographically modified nanosmooth poly (*tert*-butyl methacrylate) polymer surfaces. *Nanotechnol. Sci. Appl.* **2008**, *1*, 33–44.
60. Barbarossa, M.V.; Kuttler, C.; Fekete, A.; Rothballer, M. A delay model for quorum sensing of *Pseudomonas putida*. *BioSystems* **2010**, *102*, 148–156, doi:10.1016/j.biosystems.2010.09.001.
61. Gusnard, D.; Kirschner, R.H. Cell and organelle shrinkage during preparation for scanning electron microscopy: Effects of fixation, dehydration and critical point drying. *J. Microsc.* **1977**, *110*, 51–57, doi:10.1111/j.1365-2818.1977.tb00012.x.
62. Millikan, D.S.; Ruby, E.G. *Vibrio fischeri* flagellin A is essential for normal motility and for symbiotic competence during initial squid light organ colonization. *J. Bacteriol.* **2004**, *186*, 4315–4325, doi:10.1128/JB.186.13.4315-4325.2004.
63. Falcioni, T.; Papa, S.; Campana, R.; Manti, A.; Battistelli, M.; Baffone, W.; Bo, C. State transitions of *Vibrio parahaemolyticus* VBNC cells evaluated by flow cytometry. *Cytom. Part B Clin. Cytom.* **2008**, *74*, 272–281, doi:10.1002/cyto.b.20427.
64. Oliver, J.D.; Nilsson, L.; Kjelleberg, S. Formation of nonculturable *Vibrio vulnificus* cells and its relationship to the starvation state. *Appl. Environ. Microbiol.* **1991**, *57*, 2640–2644, doi:10.1128/aem.57.9.2640-2644.1991.
65. Oliver, J.D. The viable but non-culturable state in the human pathogen *Vibrio vulnificus*. *FEMS Microbiol. Lett.* **1995**, *133*, 203–208, doi:10.1111/j.1574-6968.1995.tb07885.x.
66. Joens, M.S.; Huynh, C.; Kasuboski, J.M.; Ferranti, D.; Sigal, Y.J.; Zeitvogel, F.; Obst, M.; Burkhardt, C.J.; Curran, K.P.; Chalasani, S.H.; et al. Helium Ion Microscopy (HIM) for the imaging of biological samples at sub-nanometer resolution. *Sci. Rep.* **2013**, *3*, 3514, doi:10.1038/srep03514.
67. Hill, R.; Notte, J.; Ward, B. The ALIS He ion source and its application to high resolution microscopy. *Phys. Procedia* **2008**, *1*, 135–141, doi:10.1016/j.phpro.2008.07.088.
68. Ward, B.W.; Notte, J.A.; Economou, N.P. Helium ion microscope: A new tool for nanoscale microscopy and metrology. *J. Vac. Sci. Technol. B* **2006**, *24*, 2871–2874, doi:10.1116/1.2357967.
69. Chang, F.; Huang, K.C. How and why cells grow as rods. *BMC Biol.* **2014**, *12*, 54, doi:10.1186/s12915-014-0054-8.
70. Ursell, T.S.; Nguyen, J.; Monds, R.D.; Colavin, A.; Billings, G.; Ouzounov, N.; Gitai, Z.; Shaevitz, J.W.; Huang, K.C. Rod-like bacterial shape is maintained by feedback between cell curvature and cytoskeletal localization. *Proc. Natl. Acad. Sci. USA* **2014**, *111*, 1025–1034, doi:10.1073/pnas.1317174111.
71. Kruse, T.; Bork-Jensen, J.; Gerdes, K. The morphogenetic MreBCD proteins of *Escherichia coli* form an essential membrane-bound complex. *Mol. Microbiol.* **2005**, *55*, 78–89, doi:10.1111/j.1365-2958.2004.04367.x.
72. Postma, J.F.; de Valk, S.; Dubbeldam, M.; Maas, J.L.; Tonkes, M.; Schipper, C.A.; Kater, B.J. Confounding factors in bioassays with freshwater and marine organisms. *Ecotoxicol. Environ. Saf.* **2002**, *53*, 226–237, doi:10.1006/eesa.2002.2195.